

# Magnetic, structural, and electronic properties of iron sulfide $\text{Fe}_3\text{S}_4$ nanoparticles synthesized by the polyol mediated process

I. S. Lyubutin · S. S. Starchikov · Chun-Rong Lin · Shin-Zong Lu ·  
Muhammad Omar Shaikh · K. O. Funtov · T. V. Dmitrieva ·  
S. G. Ovchinnikov · I. S. Edelman · R. Ivantsov

Received: 3 September 2012 / Accepted: 22 December 2012  
© Springer Science+Business Media Dordrecht 2013

**Abstract** Iron sulfide nanoparticles  $\text{Fe}_3\text{S}_4$  with the spinel-type crystal structure were synthesized by the polyol mediated process. The particle size depends on preparation conditions and varies from 9 to 20 nm. Mössbauer data have revealed that the dominating fraction of iron ions in the 9-nm sample is in the high-spin ferric state. This implies an occurrence of the

cation vacancies in nonstoichiometric greigite. The stoichiometric phase of greigite  $\text{Fe}_3\text{S}_4$  dominates in the 18-nm-size nanoparticles. Magnetic measurements have shown a ferrimagnetic behavior of all samples at temperatures between 78 and 300 K. The estimated value of magnetic moment of the stoichiometric greigite nanoparticles is about  $3.5 \mu_B$  per  $\text{Fe}_3\text{S}_4$  unit. The Mössbauer spectra indicate a superparamagnetic behavior of small particles, and some fraction of superparamagnetic phase is observed in all samples synthesized which may be caused by the particle size distribution. The blocking temperatures of  $T_B \approx 230$  and 250 K are estimated for the 9 and 14 nm particles, respectively. The Mössbauer parameters indicate a great degree of covalency in the Fe–S bonds and support the fast electron  $\text{Fe}^{3+} \rightleftharpoons \text{Fe}^{2+}$  exchange in the B-sites of greigite. An absence of the Verwey transition at temperatures between 90 and 295 K is established supporting a semimetal type of conductivity. The temperature and magnetic field dependences of the magnetic circular dichroism (MCD) of optical spectra were measured in  $\text{Fe}_3\text{S}_4$  for the first time. The spectra differ substantially from that of the isostructural oxide  $\text{Fe}_3\text{O}_4$ . It is supposed that the MCD spectra of greigite nanoparticles result from the collective electron excitations in a wide band with superimposed peaks of the  $d$ – $d$  transitions in Fe ions.

I. S. Lyubutin (✉) · S. S. Starchikov ·  
K. O. Funtov · T. V. Dmitrieva  
Shubnikov Institute of Crystallography, Russian Academy  
of Sciences, Leninsky av. 59, Moscow 119333, Russia  
e-mail: lyubutin@ns.crys.ras.ru

C.-R. Lin (✉) · S.-Z. Lu · M. O. Shaikh  
Department of Mechanical Engineering, Institute of  
Nanotechnology, Southern Taiwan University of Science  
and Technology, No. 1, Nan-Tai Street, Yungkang Dist.,  
Tainan 710, Taiwan, Republic of China  
e-mail: crlin@mail.stut.edu.tw; crlinspin@gmail.com

S. G. Ovchinnikov (✉) · I. S. Edelman · R. Ivantsov  
Kirensky Institute of Physics, Siberian Branch of Russian  
Academy of Sciences, Krasnoyarsk 660036, Russia  
e-mail: sgo@iph.krasn.ru

S. G. Ovchinnikov  
Institute of Engineering Physics and Radioelectronics,  
Siberian Federal University, Krasnoyarsk 660041, Russia

**Keywords** Iron sulfides  $\text{Fe}_3\text{S}_4$  · Magnetic and  
electronic properties · Mössbauer spectroscopy ·  
Magnetic circular dichroism

## Introduction

Greigite  $\text{Fe}_3\text{S}_4$  is a counterpart of the oxide magnetite  $\text{Fe}_3\text{O}_4$  which has been intensively studied. In the inverse spinel structure of the stoichiometric greigite  $\text{Fe}_3\text{S}_4$ , the unit cell contains 32 atoms of sulfur and 24 atoms of iron (Skinner et al. 1964; Uda 1965). There are two sublattices of iron atoms where  $\text{Fe}^{3+}$  ions occupy tetrahedral A-sites and both  $\text{Fe}^{2+}$  and  $\text{Fe}^{3+}$  ions occupy octahedral B-sites. Despite the structural similarities of  $\text{Fe}_3\text{S}_4$  and  $\text{Fe}_3\text{O}_4$ , their magnetic properties are different in many aspects (Chang et al. 2008). The room temperature saturation magnetization of the bulk greigite is  $3.13 \mu_B$  per formula unit (f.u.) while this value in magnetite is noticeably higher  $4.0 \mu_B$ . The parameter  $J_{AB}$  of exchange interaction between Fe ions in (A) and (B) sublattices in greigite, estimated recently as  $\sim 1.03$  meV, is also lower than the  $J_{AB}$  value calculated for magnetite (2.88 meV). In bulk compounds, Verwey transition (Verwey 1939) observed in magnetite is absent in greigite. Such an enumeration can be continued. The origin of the large difference between magnetic properties of  $\text{Fe}_3\text{S}_4$  and  $\text{Fe}_3\text{O}_4$  is opened to questions now.

Contrary to the bulk properties, some new features may be expected in nanoparticles related both to the individual particle properties and to the statistical behavior of a nanoparticle ensemble. In general, nanoscale magnetic structures with enhanced surface contribution are typical for both thin films (Wang et al. 2011a, b; Kumar 2010; Kumar et al. 2009) and nanoparticles in non-magnetic matrices (Gleiter 2000; Gubin et al. 2005; Chung et al. 2010). The similar properties of chalcogenide nanostructures attract considerable attention because of their fundamental and applied prospect.

Iron sulfides are of importance for geology owing to their frequent occurrence in sediments, rocks, and ore deposits (Maher and Thompson 1999), and as indicators of the gold-bearing ore presence (Menyah and O'Reilly 1991). Iron–sulfur clusters  $[\text{Fe}_2\text{S}_2]$ ,  $[\text{Fe}_3\text{S}_4]$ , and  $[\text{Fe}_4\text{S}_4]$  are found in proteins of all life forms (Beinert et al. 1997), where they undergo oxidation–reduction reactions, providing electron transfer and catalytic functions and act as sensors of iron and oxygen (Beinert et al. 1997; Surerus et al. 1989).

Iron sulfides occur in different phases: Troilite ( $\text{FeS}$ —antiferromagnetic metal), Pyrrhothite ( $\text{FeS}$ —

ferromagnetic metal), Smythite (ferromagnetic), Greigite ( $\text{Fe}_3\text{S}_4$ —ferrimagnetic semimetal), Mackinawite ( $\text{Fe}_{1+x}\text{S}$  paramagnetic metal), Marcasite ( $\text{FeS}_2$ —diamagnetic semiconductor), Pyrite ( $\text{FeS}_2$ —diamagnetic semiconductor) (Hobbs and Hafner 1999). In contrast to iron oxides the phase diagram of iron sulfides is more complicated and thus variation in the relation of Fe and S atoms and temperature of reaction allows creating samples with different structural, electrical, and magnetic properties.

In nature  $\text{Fe}_3\text{S}_4$  can be identified in anoxic marine and lake sedimentary systems (Roberts and Weaver 2005). It can be used in paleomagnetic and environmental magnetic studies (Maher and Thompson 1999; Snowball and Thompson 1988, 1990; Roberts et al. 1996; Jiang et al. 2001; Rowan and Roberts 2006; Babinski et al. 2007; Vasiliev et al. 2007), as a precursor to pyrite in the Fe–S system, in the pyritization process and in Fe–S geochemistry (Benning et al. 2000; Hunger and Benning 2007). Also, magnetotactic bacteria can produce greigite magnetosomes (Posfai et al. 1998). Magnetic properties of greigite are very sensitive to the sample preparation conditions and remain poorly understood up to now (see recent review by Roberts et al. 2011).

Greigite nanoparticles were synthesized by several authors with different techniques (Chang et al. 2010; Vasilenko et al. 2010). Magnetism of  $\text{Fe}_3\text{S}_4$  nanoparticles was studied by static magnetization measurements (Zhang and Chen 2009; Vasilenko et al. 2010). Properties of nanoparticle ensembles varied in wide ranges depending on the fabrication peculiarities. However, the relevant Mössbauer spectroscopy data on the size effect on magnetic properties were not obtained. Magneto-optical measurements of greigite are also absent in the literature.

We expect that the complex studies of the nanoparticles properties for different particle size and sample preparation conditions will bring new fundamental information and give impetus to new applications. In the present work the  $\text{Fe}_3\text{S}_4$  nanoparticles were synthesized by heating iron acetate and thiourea in diethylene glycol. The X-ray diffraction, Mössbauer spectroscopy, magnetic, and magneto-optic measurements reveal that structural, magnetic, and electronic properties of the nanoparticles strongly depend on the particle size and sample preparation conditions.

## Sample preparation and methods of characterization

Several samples of the  $\text{Fe}_3\text{S}_4$  nanoparticles were synthesized by the polyol mediated process. The polyol process, which exploits high-boiling polyalcohol solvents [e.g., glycerol, diethylene glycol (DEG), ethylene glycol, tetraethylene glycol] that also act as mild reducing agents when heated, was originally developed for the synthesis of nanocrystalline powders of Pd and other late transition elements. To synthesize  $\text{Fe}_3\text{S}_4$  nanoparticles by polyol method, the reaction temperature must be higher than 170 °C. We choose DEG as a reaction solvent because of its' high boiling point (240 °C). It is a one-pot method involving the reaction of stable precursors and solvent [iron (II) acetate ( $\text{Fe}(\text{COOCH}_3)_2$ ) as the cation source, thiourea ( $\text{NH}_2\text{CSNH}_2$ ) as the sulfur source, and diethylene glycol (DEG) as the solvent]. With polyvinylpyrrolidone powder (PVP) as a capping agent,  $\text{Fe}_3\text{S}_4$  nanocrystals were produced under a mild temperature while high pressure was not required. Typically, 0.7 g of  $\text{Fe}(\text{COOCH}_3)_2$ , 5.0 g of PVP (with average MW = 58000), 0.62–1.53 g of  $\text{NH}_2\text{CSNH}_2$ , and 50 ml of DEG were added into a three-neck round-bottom flask equipped with a magnetic stirrer and an inlet of argon gas. Then the mixture was heated with stirring to refluxing temperature between 180 and 220 °C for 2–5 h. After cooling to room temperature a black colloid suspension containing PVP-coated  $\text{Fe}_3\text{S}_4$  nanocrystals were formed. The nanocrystals can be separated from the suspension with a magnetic field. To remove excess polyol and complete the process, the nanocrystals were washed several times with ethanol by magnetic decantation. In general, the crystallite sizes of  $\text{Fe}_3\text{S}_4$  nanocrystals could be

controlled via the relative concentration of iron sources and sulfur sources, reaction time, and reaction temperatures. To change the crystallite size, we found that the reactive sources (Fe/S mol. ratio) are more effective than the heating temperature and reaction times. The details of the process of the selected samples are described and summarized in Table 1.

The crystal structure and phase purity of the samples were examined by X-ray powder diffraction (XRD). As shown in Fig. 1, all reflections can be readily indexed to the cubic phase with spinel-type structure (space group  $Fd\bar{3}m$ ). The estimation of the crystallite size by the Scherrer's formula due to the peak broadening (Langford and Wilson 1978) gives an average size  $D$  from 9 to 20 nm (Table 1). The particles shape and size were examined by the

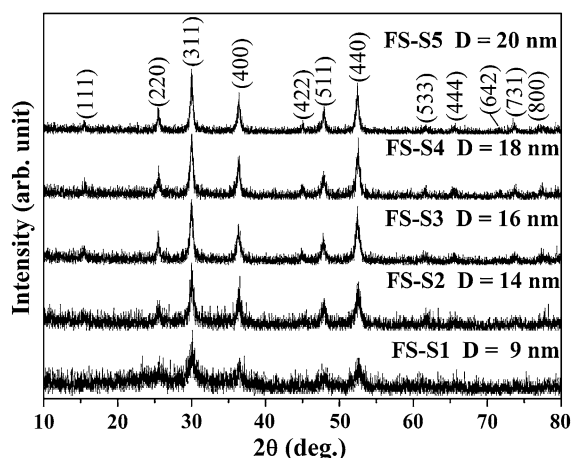


**Fig. 1** Room temperature X-ray diffraction patterns of the iron sulfide nanoparticles recorded for the samples prepared at different conditions shown in Table 1. The reflection indexes correspond to the cubic spinel-type structure of  $\text{Fe}_3\text{S}_4$  (sp. gr.  $Fd\bar{3}m$ )

**Table 1** Some details of the synthesis of the iron sulfide  $\text{Fe}_3\text{S}_4$  nanoparticles

Sample name	Fe/S (mol. ratio)	Reaction scheme	Crystal structure	$D$ (nm)	$A$ (%) ( $\pm 2$ )
FS-S1	1/2	$\text{Fe}(\text{COOCH}_3)_2 + \text{thiourea} + \text{DEG} + \text{PVP} \rightarrow 200\text{ }^\circ\text{C}; 2.5\text{ h}$	Spinel	9	12
FS-S2	1/2.5	$\text{Fe}(\text{COOCH}_3)_2 + \text{thiourea} + \text{DEG} + \text{PVP} \rightarrow 200\text{ }^\circ\text{C}; 2.5\text{ h}$	Spinel	14	38
FS-S3	1/3	$\text{Fe}(\text{COOCH}_3)_2 + \text{thiourea} + \text{DEG} + \text{PVP} \rightarrow 200\text{ }^\circ\text{C}; 2.5\text{ h}$	Spinel	16	37
FS-S4	1/3	$\text{Fe}(\text{COOCH}_3)_2 + \text{thiourea} + \text{DEG} + \text{PVP} \rightarrow 220\text{ }^\circ\text{C}; 4.5\text{ h}$	Spinel	18	64
FS-S5	1/5	$\text{Fe}(\text{COOCH}_3)_2 + \text{thiourea} + \text{DEG} + \text{PVP} \rightarrow 180\text{ }^\circ\text{C}; 4.5\text{ h}$	Spinel	20	52

Fe/S is the molar ratio of  $\text{Fe}(\text{COOCH}_3)_2$  to thiourea.  $D$  is the average size of the nanoparticles.  $A$  is the abundance of stoichiometric greigite  $\text{Fe}_3\text{S}_4$  phase (relative to Fe content) obtained from the Mössbauer data

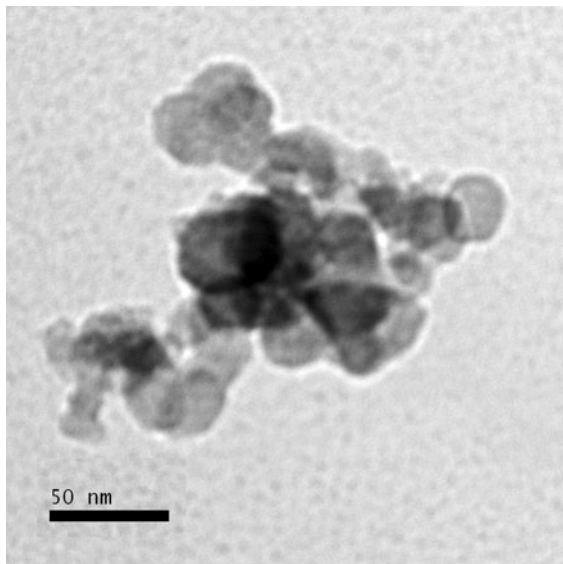


**Fig. 2** The transmission electron microscopy images of the  $\text{Fe}_3\text{S}_4$  nanoparticles

transmission electron microscopy (TEM), and a plate form of the 9 nm sample can be seen in the TEM images shown in Fig. 2.

The Mössbauer spectroscopy was applied to examine the phase composition, structural, magnetic, and electronic properties of the nanoparticles. The  $^{57}\text{Fe}$ -Mössbauer spectra were recorded at temperatures 90 and 295 K in the transmission geometry with a standard spectrometer operating in the constant accelerations regime. The gamma-ray source  $^{57}\text{Co}(\text{Rh})$  was at room temperature, and the isomer shifts were measured relative to metal  $\alpha\text{-Fe}$  at room temperature. The magnetic measurements were performed at temperatures between 78 and 300 K using the VSM-type magnetometer (vibrating sample magnetometer) in an applied field sweeping from  $-11$  to  $11$  kOe.

To our knowledge, the greigite magneto-optical properties have been investigated neither for bulk nor for nanoparticle samples, that can be associated, partly, with the opaqueness of the both types of samples. For our magneto-optical measurements of  $\text{Fe}_3\text{S}_4$  the transparent nanocomposites based on the non-magnetic matrix with embedded  $\text{Fe}_3\text{S}_4$  nanoparticles of  $\sim 20$  nm in size have been prepared (FS-5 in Table 1). In the preparation process the vacuum lubricant (mineral oil mixed with ceresin and caoutchouc, in Russia State Standard: 9645—61) was chosen as a material for the matrix. The lubricant was slightly heated to liquid

state, and then the  $\text{Fe}_3\text{S}_4$  powder was added and mixed inside it. The obtained paste was placed between two polished glass plates which were pressed to each other. After cooling to room temperature the samples were transparent in visible spectral range. Several samples of different thickness  $D$  were prepared:  $\sim 0.08$  mm (FS-5.1),  $\sim 0.001$  mm (FS-5.2),  $\sim 0.02$  mm (FS-5.3). Besides, petrolatum oil was used as a material for the matrix (sample # FS-5.4 with  $D \sim 0.001$  mm). So, properties of all samples FS-5.1–FS-5.4 should be compared with that of FS-5 nanopowder (Table 1). In our pioneering magneto-optical study a fixed nanoparticle size was chosen; the size dependence of the effect will be investigated in the nearest future. Thin magnetite  $\text{Fe}_3\text{O}_4$  films were prepared for the comparative measurements.

The magnetic circular dichroism (MCD) spectra were measured using the modulation of light polarization with a piezoelectric modulator (Jasperson and Schnatterly 1969). The modulator consisted of the piezoelectric ceramic element pasted on the plate of fused silica. The modulator was a part of the self-contained generator and oscillated with its resonance frequency of about 25 kHz. The light beam from the filament lamp passing through the polarizer and then through the modulator became circularly polarized, and the light polarization changes from right circular to left circular one with the resonance frequency of the modulator. The circularly polarized light passing through the sample placed between magnetic poles acquires a modulation of its intensity due to circular dichroism of the sample. The MCD effect was measured with a relative accuracy of  $10^{-4}$  as a difference in photomultiplier signals (proportional to the light intensity change) obtained at the magnetic field applied along and opposite to the light direction. The measurements were performed in the spectral region 300–1000 nm over the temperature range 100–295 K in magnetic fields up to 0.55 T.

## Results of magnetic, Mössbauer, and magneto-optic spectroscopy measurements

### Magnetic measurements

Magnetization curves of all samples reveal a ferromagnetic (or ferrimagnetic) behavior at temperatures between 78 and 300 K (Fig. 3). In a relatively low

applied field  $H_{\text{ext}}$  the magnetization sharply increases showing a “soft” magnetic behavior, and it almost approaches saturation at 10 kOe. The insets in Fig. 3a–d show the zoomed view of hysteresis plots for different particle size, whereas the temperature and size dependences of coercivity  $H_C$ , remanence magnetization  $M_r$ , and saturation magnetization  $M_S$  are given in Fig. 4a, b, respectively. At room temperature the value of saturation magnetization  $M_S$  (extrapolated to  $H_{\text{ext}} = 0$ ) is the highest for the 20 nm particles size ( $M_S \approx 44$  emu/g) while it is the smallest ( $M_S \approx 9$  emu/g) for the 9-nm particles size. These values are below the 59 emu/g value found for high-quality synthetic bulk (14  $\mu\text{m}$ ) greigite (Chang et al. 2008), but the 20-nm particle’s value is close to the hydrothermally synthesized greigite with  $M_S \sim 40$  emu/g (Wang et al. 2011a, b).

For the 20-nm-size particles the  $M_S$  value extrapolated to 0 K is about 48 emu/g which corresponds to  $\approx 2.7 \mu_B$  per  $\text{Fe}_3\text{S}_4$  unit. Taking into account the Mössbauer data (which reveal that 30 % of Fe atoms in this FS-S5 sample are paramagnetic at 90 K), the corrected value of magnetic moment of the 20 nm size particle is about  $3.5 \mu_B$  per  $\text{Fe}_3\text{S}_4$  unit. This value is higher than that in bulk greigite ( $\approx 3.0 \mu_B$ ) found

recently from the neutron diffraction data (Chang et al. 2009).

With temperature rise from 78 to 300 K, the  $M_r$  and  $H_C$  values gradually decrease for all particle sizes while the  $M_S$  value is practically stable (Fig. 4a). At the temperature fixed at 78 K, the  $M_S$  value strongly increases with the particle size increasing (Fig. 4b). The  $M_r$  value is only slightly increased whereas the  $H_C$  behavior is not regular.

Temperature dependences of the field-cooled (FC) and zero-field-cooled (ZFC) magnetizations are shown in Fig. 5. The ZFC and FC curves measured in the low field of  $H_{\text{ext}} = 0.5$  kOe are split below  $T_{\text{int}} \approx (250\text{--}300)$  K implying an appearance of magnetic interactions between nanoparticles (Lotgering 1964). In the high field 11 kOe these anomalies are not observed down to 78 K. The ZFC curves of 9 and 14 nm particles measured in the field of 0.5 kOe display a maximum at  $T_B \approx 230$  and 250 K, respectively. This behavior is typical for systems of magnetic moments which undergo a spin blocking (or frozen) effect. Above blocking temperature  $T_B$  particles are in superparamagnetic state while below  $T_B$  thermal fluctuations of magnetic moments are blocked by magnetic anisotropy. For the larger particle size the  $T_B$

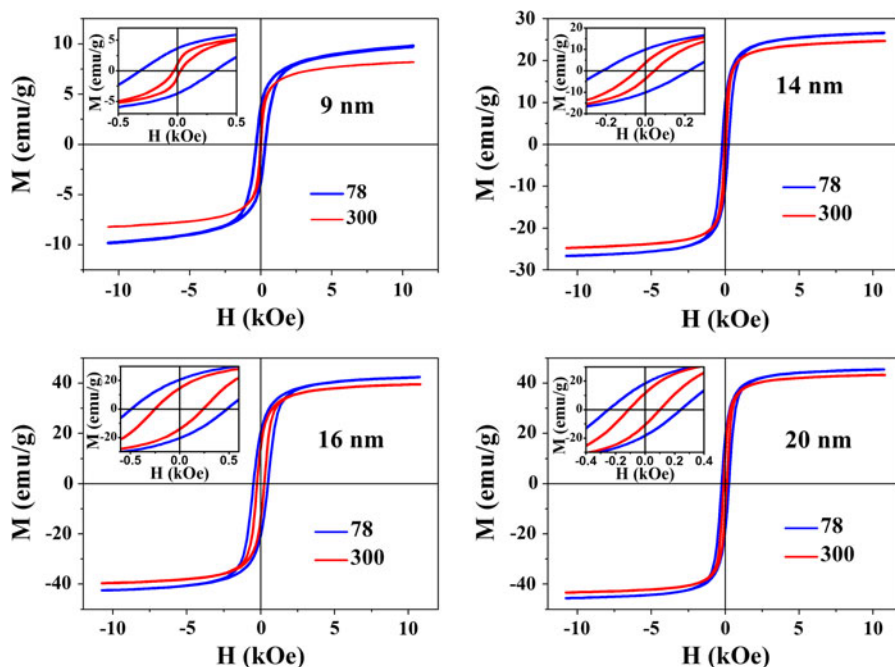


**Fig. 3** The magnetic applied field dependences of magnetization and hysteresis loops recorded at 78 and 300 K for the  $\text{Fe}_3\text{S}_4$  nanoparticles with different particle size. *Inserts* show the zoomed view of hysteresis plots



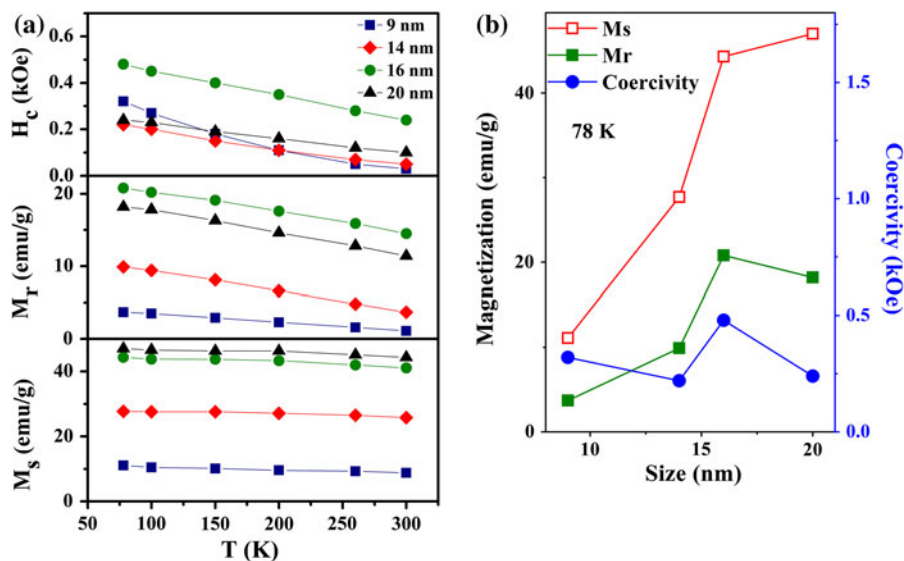


**Fig. 4** **a** Temperature dependences of the saturation magnetization  $M_s$ , remanence magnetization  $M_r$ , and coercivity  $M_c$  for the  $\text{Fe}_3\text{S}_4$  nanoparticles with different particle size. **b** The size

dependence of the  $M_s$ ,  $M_r$ , and  $M_c$  parameters obtained at 78 K. Solid lines are guides for the eye

value is above room temperature. As we show below, Mössbauer spectra indicate a superparamagnetic behavior of small particles, and some fraction of superparamagnetic state is observed in all samples synthesized which may be caused by the particle size distribution.

#### Mössbauer spectroscopy data

The representative  $^{57}\text{Fe}$ -Mössbauer spectra recorded at 90 and 295 K for all samples are shown in Fig. 6a, b. All spectra consist of six-line magnetic patterns and a central doublet typical of a paramagnetic iron state. The line widths of the doublet and magnetic pattern are rather broad due to several overlapping components corresponding to nonequivalent states of iron ions. The central doublet is most intensive (dominating) in the sample with small particles (9 nm) and it decreases with increasing the particle size (Fig. 6).

The spectra for the 9-nm sample (Fig. 7a) revealed that the central doublet consists of two doublet components with almost equal isomer shift value  $\delta \approx 0.37$  mm/s but with different quadrupole splitting  $\varepsilon = 0.64$  and 1.08 mm/s (at 295 K) (Table 2). The similar component with  $\varepsilon = 0.64$  mm/s was found in (Morice et al. 1969; Spender et al. 1972) and it seems that it is typical of greigite small particles with a wide size distribution. At 295 K the total area of

this paramagnetic component in the 9-nm sample is about 86 % of the total iron content and it slightly decreases (to 78 %) at 90 K. The observed isomer shift value clearly indicates that the dominating fraction of iron ions in the 9-nm sample is in the high-spin ferric state. This is not consistent with a stoichiometric  $\text{Fe}_3\text{S}_4$ . Taking into account the XRD data showing the spinel-type crystal structure (Fig. 1) in all samples, we have to conclude an occurrence of the cation vacancies in small particles of nonstoichiometric greigite. Most probably in small particles (<9 nm) all iron ions are oxidized to ferric state and a vacant  $\text{Fe}_2\text{S}_3$  spinel-type structure appears analogous to the oxide maghemite  $\gamma\text{-Fe}_2\text{O}_3$  structure. In these cases the cation vacancies  $\square$  occur in the octahedral B-sites of the spinel ( $\text{Fe}[\text{Fe}_{5/6}\square_{1/6}]_2\text{X}_4$  (here X = S or O), and iron ions are in the ferric  $\text{Fe}^{3+}$  state in both tetrahedral (A) and octahedral [B] sites.

The idea of occurrence of the vacant  $\text{Fe}_2\text{S}_3$  spinel-type structure (we call it as the  $\gamma\text{-Fe}_2\text{S}_3$  phase by analogy with maghemite) is also supported by the intensity ratio of the Mössbauer components corresponding to the (A) and [B] sites (Table 2). In the stoichiometric  $\text{Fe}_3\text{S}_4$ , the intensity ratio of the (A) and [B] Mössbauer components must be close to 1:2, while in the vacant  $\gamma\text{-Fe}_2\text{S}_3$  it is expected to be near 1:1.67. The observed A/B ratio in  $\gamma\text{-Fe}_2\text{S}_3$  is about 1.62 (Table 2) that is close to the expected value. The X-ray

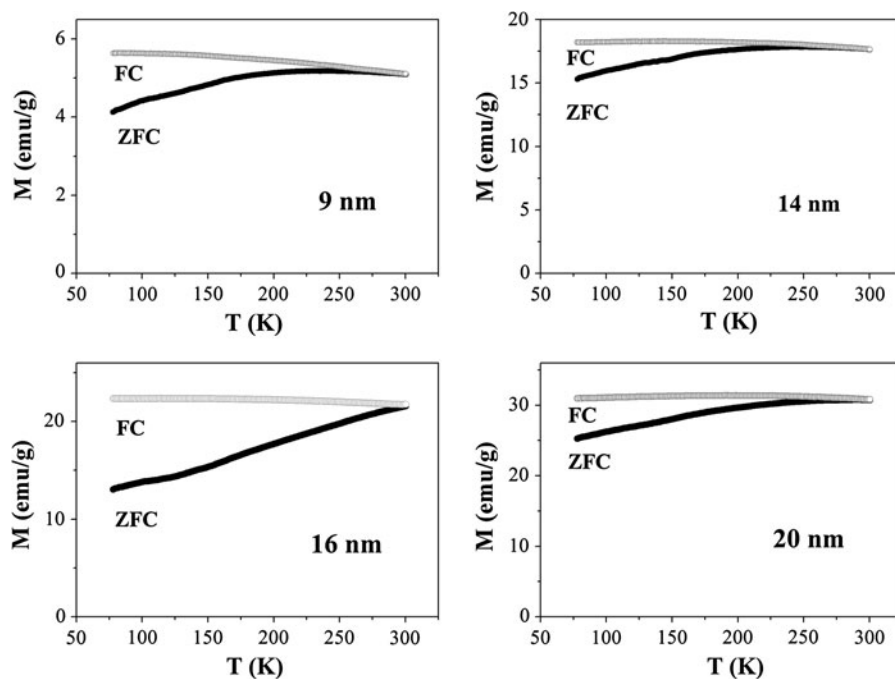


**Fig. 5** Temperature dependences of the ZFC and FC magnetization for the  $\text{Fe}_3\text{S}_4$  nanoparticles with different particle size

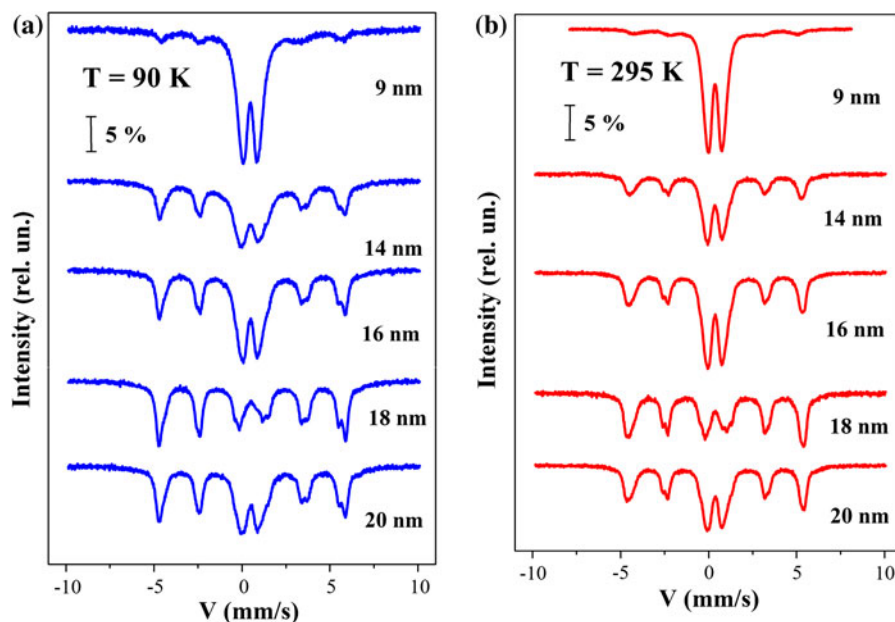


**Fig. 6** The  $^{57}\text{Fe}$ -Mössbauer spectra of greigite  $\text{Fe}_3\text{S}_4$  nanoparticles with different particle size at temperatures 90 (a) and 295 K (b)

diffraction patterns indicate a random distribution of vacancies through the crystal because extra reflections are absent. We note that the spinel-type  $\text{Fe}_2\text{S}_3$  compound containing vacancies was synthesized in

an acidic medium by Yamaguchi and Wada (1973). The authors concluded that greigite, prepared chemically and known in nature, often corresponded to a solid solution  $\text{Fe}_3\text{S}_4\text{--Fe}_2\text{S}_3$ .

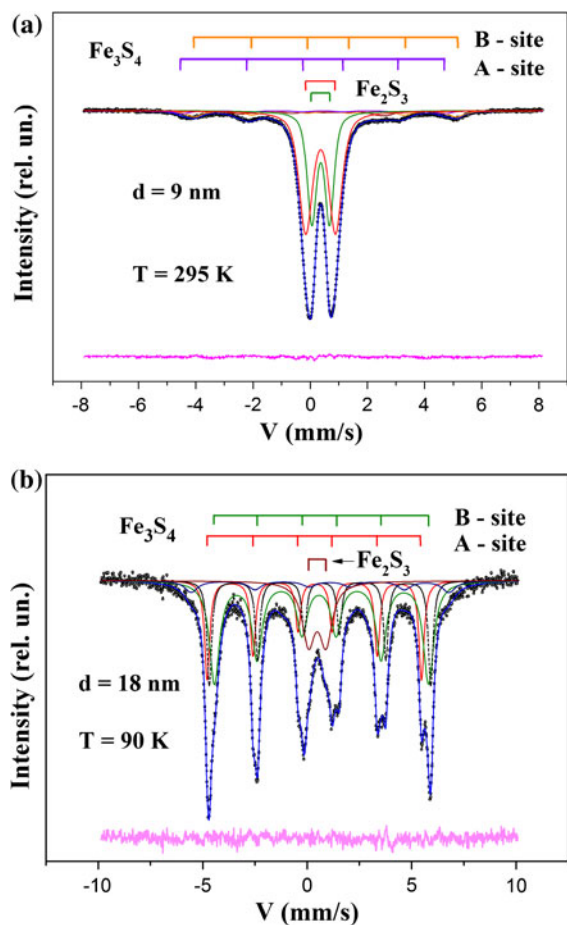


**Fig. 7** The  $^{57}\text{Fe}$ -Mössbauer spectra of the greigite nanoparticles with the particle size 9 nm at temperature 295 K (a) and 18 nm at 90 K (b). The spectra fitting to magnetic and paramagnetic components attributed to nonequivalent iron sites in  $\text{Fe}_3\text{S}_4$  and  $\text{Fe}_2\text{S}_3$  are shown by grid-ticks above the spectra. Lines at the bottom are the misfit deviation signal

It is evident from the Mössbauer data that the small  $\text{Fe}_2\text{S}_3$  nanoparticles are paramagnetic down to 90 K due to superparamagnetic effect. A small fraction of the magnetic component visible in the Mössbauer spectra (see Fig. 6; Table 2) and in magnetic measurements of 9-nm sample is originated from the particles with larger size due to the size distribution effect.

The intensity of six-line magnetic patterns in Mössbauer spectra increases with larger particle size and the magnetic components dominate in the 18 nm—size particles of sample FS-S4 (Figs. 6, 7b). The spectra processing reveals three magnetic components corresponding to iron ions in different structural and electronic states. An example of the spectra

fitting is shown in Fig. 7b, and the values of all hyperfine parameters are given in Table 3.

Considering the obtained hyperfine parameters and taking into account the data of previous studies of the natural and synthetic greigite (Chang et al. 2008; Morice et al. 1969; Spender et al. 1972; Coey et al. 1970; Stanjek and Murad 1994), we found that two of three magnetic components belong to the stoichiometric  $\text{Fe}_3\text{S}_4$ . The line-intensity ratio of these two components is close to 1:2 (Table 3). The isomer shift values  $\delta(295\text{ K}) = 0.27\text{ mm/s}$  and  $\delta(90\text{ K}) = 0.36\text{ mm/s}$  are typical of the high-spin ferric ions in the tetrahedral A-site of the spinel structure, while the values  $\delta(295\text{ K}) = 0.53\text{ mm/s}$  and  $\delta(90\text{ K}) = 0.63\text{ mm/s}$  are characteristic of ferrous ions in the octahedral B-site. The values of magnetic hyperfine fields  $H_{\text{hf}}$  at iron nuclei are close for octahedral and tetrahedral sites and are in the range of (31.9–30.0) Tesla at temperatures between 90 and 295 K (Table 3). These  $H_{\text{hf}}$  values in sulfides are much lower than in oxides (typically 50–55 T) which is explained by delocalization of  $d$  electrons in sulfides with reduction of the ionic magnetic moment of iron (Spender et al. 1972; Coey et al. 1970). The relative content of the stoichiometric  $\text{Fe}_3\text{S}_4$  greigite calculated from the Mössbauer data is given in Table 1 for all samples synthesized. The highest  $\text{Fe}_3\text{S}_4$  abundance of about 64 % is found in the FS-S4 sample with  $d = 18\text{ nm}$  (Table 1).

In all samples the third magnetic Mössbauer component was found with the hyperfine parameters typical of ferrous iron ions. The isomer shift values  $\delta$  of this component are 0.52 and 0.66 mm/s at 295 and 90 K, respectively, while the magnetic hyperfine fields  $H_{\text{hf}}$  are 31.0 and 32.9 T at 295 and 90 K, respectively. In all samples, the relative content of this component is approximately stable at about (15–17 %) of the total iron content. It can be suggested that this component belongs to the smythite phase which has the same chemical formula as greigite,  $\text{Fe}_3\text{S}_4$ , but all iron is ferrous (Makarov et al. 1969; Hoffmann et al. 1993).

#### Magnetic circular dichroism in optical spectra

As it was mentioned in section “[Sample preparation and methods of characterization](#),” the MCD measurements have been performed for several transparent samples containing nanoparticles of the same size,  $\sim 20\text{ nm}$  (FS-5 in Table 1). According to the FC-ZFC magnetization (Fig. 5) and Mossbauer data (Fig. 6),



**Table 2** Hyperfine parameters obtained from the  $^{57}\text{Fe}$ -Mössbauer spectra at 295 and 90 K for the  $d = 9$  nm size nanoparticles of greigite

Iron component	$\delta$ (mm/s) ( $\pm 0.01$ )	$\varepsilon$ (mm/s) ( $\pm 0.01$ )	$H_{\text{hf}}$ (T) ( $\pm 0.2$ )	$S$ (%) ( $\pm 2$ )	$\Gamma$ (mm/s) ( $\pm 0.02$ )
295 K					
$\text{Fe}^{3+}$ in tetrahedral A-sites of $\gamma\text{-Fe}_2\text{S}_3$	0.37	0.62	–	34	0.40
$\text{Fe}^{3+}$ in octahedral B-sites of $\gamma\text{-Fe}_2\text{S}_3$	0.37	1.05	–	55	0.55
$\text{Fe}^{3+}$ in tetrahedral A-sites of $\text{Fe}_3\text{S}_4$	0.27	–0.35	28.5	4	0.58
$\text{Fe}^{2.5+}$ in octahedral B-sites of $\text{Fe}_3\text{S}_4$	0.56	–0.09	28.4	7	0.65
90 K					
$\text{Fe}^{3+}$ in tetrahedral A-sites of $\gamma\text{-Fe}_2\text{S}_3$	0.47	0.65	–	31	0.42
$\text{Fe}^{3+}$ in octahedral B-sites of $\gamma\text{-Fe}_2\text{S}_3$	0.47	1.12	–	50	0.62
$\text{Fe}^{3+}$ in tetrahedral A-sites of $\text{Fe}_3\text{S}_4$	0.39	–0.08	31.3	7	0.60
$\text{Fe}^{2.5+}$ in octahedral B-sites of $\text{Fe}_3\text{S}_4$	0.66	–0.09	31.9	12	0.78

$H_{\text{hf}}$  is the magnetic hyperfine field at  $^{57}\text{Fe}$  nuclei,  $\delta$  is the isomer shift relative to  $\alpha\text{-Fe}$  at room temperature,  $\varepsilon$  is the quadrupole shift,  $S$  is the relative line area of the spectrum component, and  $\Gamma$  is the half maximum line width.  $\gamma\text{-Fe}_2\text{S}_3$  is the nonstoichiometric greigite with the spinel structure and  $\text{Fe}_3\text{S}_4$  is the stoichiometric greigite

**Table 3** Hyperfine parameters obtained from the  $^{57}\text{Fe}$ -Mössbauer spectra at 295 and 90 K for the  $d = 18$  nm size nanoparticles of greigite  $\text{Fe}_3\text{S}_4$ 

Iron component	$\delta$ (mm/s) ( $\pm 0.01$ )	$\varepsilon$ (mm/s) ( $\pm 0.01$ )	$H_{\text{hf}}$ (T) ( $\pm 0.2$ )	$S$ (%) ( $\pm 2$ )	$\Gamma$ (mm/s) ( $\pm 0.02$ )
295 K					
$\text{Fe}^{3+}$ in tetrahedral A-sites of $\text{Fe}_3\text{S}_4$	0.27	–0.01	30.9	22	0.29
$\text{Fe}^{2.5+}$ in octahedral B-sites of $\text{Fe}_3\text{S}_4$	0.53	0.09	30.0	42	0.57
$\text{Fe}^{2+}/\text{Fe}^{2.5+}$ ions in smythite	0.52	–0.09	31.0	17	0.26
Paramagnetic $\text{Fe}^{3+}$ ions in $\gamma\text{-Fe}_2\text{S}_3$	0.37	0.86	–	19	0.55
90 K					
$\text{Fe}^{3+}$ in tetrahedral A-sites of $\text{Fe}_3\text{S}_4$	0.36	–0.04	31.9	23	0.30
$\text{Fe}^{2.5+}$ in octahedral B-sites of $\text{Fe}_3\text{S}_4$	0.63	0.12	31.8	45	0.59
$\text{Fe}^{2+}/\text{Fe}^{2.5+}$ ions in smythite	0.66	–0.09	32.9	19	0.27
Paramagnetic $\text{Fe}^{3+}$ ions in $\gamma\text{-Fe}_2\text{S}_3$	0.48	0.84	–	13	0.73

$H_{\text{hf}}$  is the magnetic hyperfine field at  $^{57}\text{Fe}$  nuclei,  $\delta$  is the isomer shift relative to  $\alpha\text{-Fe}$  at room temperature,  $\varepsilon$  is the quadrupole shift,  $S$  is the relative line area of the spectrum component, and  $\Gamma$  is the half maximum line width

these nanoparticles in the powder state have frozen magnetic moments at the room temperature. Besides size effects should be minimal for these nanoparticles compared to nanoparticles of a smaller size. So magneto-optical properties of the composite containing larger nanoparticles should be closer to the properties of the bulk greigite which is desirable for the first magneto-optical investigation of the matter. We found that the MCD dependence on applied magnetic field appeared to coincide totally with the magnetization hysteresis loop of the 20 nm sample

(Fig. 3) independent of the samples FS-5.1–FS-5.4 thickness. An example of the MCD hysteresis loop is shown in Fig. 8 for the sample FS-5.1. This observation confirms the MCD origin from the ferrimagnetic phase of greigite. The room temperature MCD spectra are shown in Fig. 9. The spectra shape is seen to be similar for all samples FS-5.1–FS-5.4. The wide positive maximum centered at  $\sim 400\text{--}700$  nm is the main peculiarity of the spectrum. Additional weak features are seen at about 400 and 620 nm against a background of this maximum. Their intensities

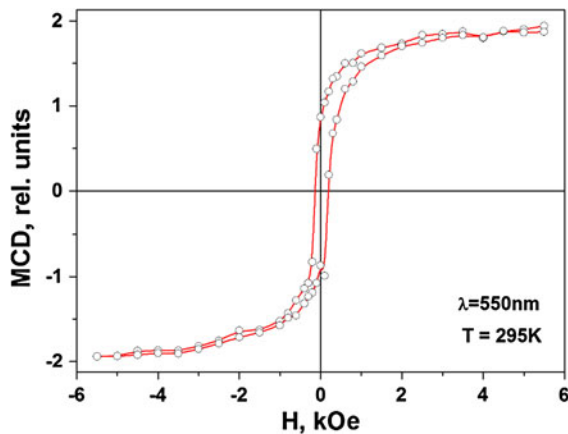


**Fig. 8** Room temperature MCD value vs external magnetic field  $H$  for the greigite nanoparticles with size 20 nm (sample #1)

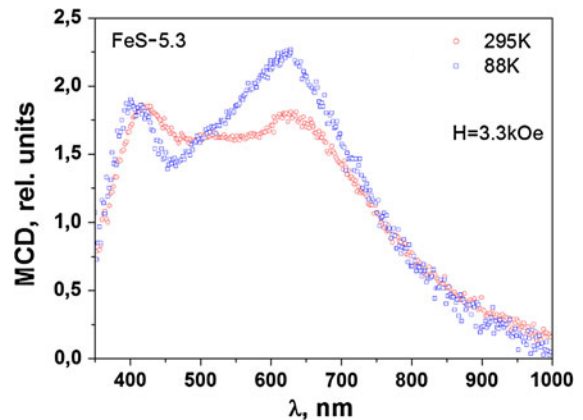


**Fig. 10** MCD spectra for the greigite nanoparticles with size 20 nm (sample #3) for two temperatures in external magnetic field 3 kOe

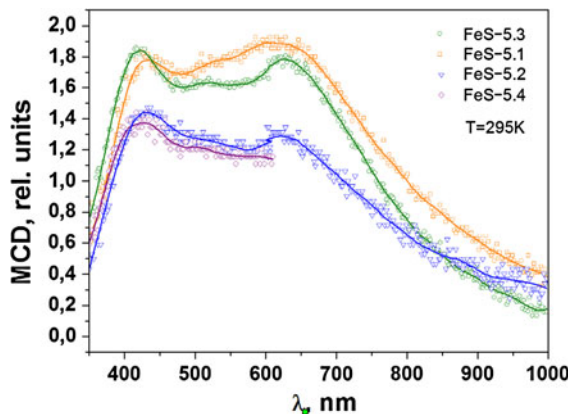


**Fig. 9** Room temperature MCD spectra for the greigite nanoparticles with size 20 nm (sample #1, #2, #4) in magnetic field 5.5 kOe and for the sample #3 in the field 3 kOe

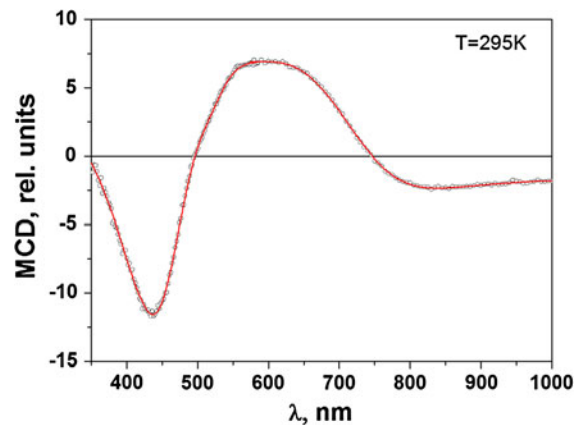


**Fig. 11** Room temperature MCD spectrum of the  $\text{Fe}_3\text{O}_4$  film on the glass substrate

increase slightly with temperature decreasing (Fig. 10).

In the absence of any data on the MCD measurements in  $\text{Fe}_3\text{S}_4$ , the comparison with the MCD spectrum for the isostructural oxide  $\text{Fe}_3\text{O}_4$  (Fig. 11) seems to be reasonable. The comparison (see Figs. 9, 10, and 11) clearly indicates the great difference between these compounds, in spite of the total similarity of  $\text{Fe}_3\text{O}_4$  and  $\text{Fe}_3\text{S}_4$  both in structure (spinel) and in assumed  $\text{Fe}^{3+}$  and  $\text{Fe}^{2+}$  ion distribution among the octahedral and tetrahedral sites.

Two extremes of opposite sign are seen in the visible magnetite thin film MCD spectrum that corresponds totally to the magnetite MCD spectrum

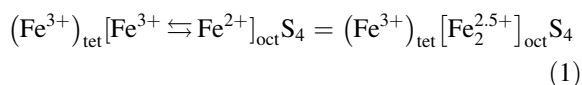
observed by Gehring et al. (2012). Analogous features were characteristic of the magneto-optical polar Kerr effect spectrum of bulk magnetite sample (Fontijn et al. 1997). These spectrum peculiarities were ascribed to the charge transfer electron transitions between Fe ions of different valence or occupying different crystal positions (Fontijn et al. 1997). Evidently, another mechanism should be invoked to understand the origin of the greigite MCD spectrum.

## Discussion

As shown by Mössbauer spectra measurements in an applied magnetic field (Chang et al. 2008; Spender

et al. 1972; Coey et al. 1970),  $\text{Fe}_3\text{S}_4$  is a ferrimagnet with collinear antiparallel ordering of iron magnetic moments of A and B sublattices (the Neel spin configuration). In the compound with an inverse cation distribution  $(\text{Fe}^{3+})_{\text{tet}}[\text{Fe}^{3+}\text{Fe}^{2+}]_{\text{oct}}\text{S}_4$ , the magnetic moment  $M$  is too small to be accounted for by a purely ionic model which implies  $M = 4 \mu_{\text{B}}$  for the spin magnetic moment of the formula unit (Coey et al. 1970; Dekkers et al. 2000). It is explained by partial delocalization of  $3d$  electrons leading to semimetallic properties of greigite which are supported by the conductivity measurement (Spender et al. 1972) and theoretical calculations (Devey et al. 2009).

The isomer shifts are generally rather smaller in sulfides than in oxides due to the larger degree of covalency of the Fe–S bonds. In particular, the  $\delta$  values in both A- and B-sites of greigite  $\text{Fe}_3\text{S}_4$  are smaller than the corresponding values in oxide  $\text{Fe}_3\text{O}_4$ . In our stoichiometric  $\text{Fe}_3\text{S}_4$  nanoparticles the A-site isomer shift  $\delta(295 \text{ K}) = 0.27 \text{ mm/s}$  suggests that the iron on these sites is predominantly ferric. The B-site isomer shift value  $\delta(295 \text{ K}) = 0.52 \text{ mm/s}$  is quite consistent with the presence of both ferric and ferrous ions on these sites, if we assume that fast electronic exchange occurs between the two species. Due to fast electron hopping between  $\text{Fe}^{2+}$  and  $\text{Fe}^{3+}$  ions in the B-sites, the average iron valence is near  $\text{Fe}^{2.5+}$  (Spender et al. 1972; Coey et al. 1970).



The Mössbauer spectra do not distinguish the  $\text{Fe}^{2+}$  and  $\text{Fe}^{3+}$  ions in B-sites thus supporting the fast electron  $\text{Fe}^{3+} \rightleftharpoons \text{Fe}^{2+}$  exchange. The magnetic field  $H_{\text{hf}}$  in the B-sites is somewhat lower than in the A-sites and this is consistent with the iron valence states.

The magnetization measurements of our nanoparticles show no abrupt changes at low temperatures down to 78 K, so it is unlikely that the Verwey transition has occurred. This conclusion is in agreement with (Roberts et al. 2011). The shapes of Mössbauer spectra and the hyperfine parameters support an absence of the Verwey transition at temperatures between 90 and 295 K (Lyubutin et al. 2009). At the Verwey transition in magnetite, the spinel structure transforms into the low-temperature monoclinic structure (Piekarz et al. 2007). However, as shown by the theoretical simulations (using the

GGA+U approach) (Devey et al. 2009), the monoclinic structure of greigite could be stable with respect to the spinel structure only at high values of the Hubbard parameter  $U_{\text{eff}} > 5 \text{ eV}$  (representing the electron correlations associated with the Fe atoms in greigite), which is not consistent with physical properties (electronic and magnetic) of greigite. As shown in (Devey et al. 2009) the covalent admixture of the Fe–S bonds, being more pronounced than that of the more ionic Fe–O bonds, results in the smaller value of the electron correlation parameter  $U_{\text{eff}}$  in thiospinel. In particular, a semimetal type of conductivity is predicted in greigite at  $U_{\text{eff}} = 1 \text{ eV}$  (Devey et al. 2009).

Possibly, the covalent character of Fe–S bonds is also responsible for the strong difference between the MCD spectra of  $\text{Fe}_3\text{S}_4$  and  $\text{Fe}_3\text{O}_4$ . The difference in lattice parameters can also contribute to such a MCD behavior. Indeed, the parameter  $a$  for  $\text{Fe}_3\text{S}_4$  is (9.8718–9.8734) Å (Chang et al. 2009) and 8.3941(7) Å in  $\text{Fe}_3\text{O}_4$  (Fleet 1981). The higher electric conductivity of  $\text{Fe}_3\text{S}_4$  compared to that of  $\text{Fe}_3\text{O}_4$  should also be taken into account. Considering these factors, the wide peak ranging from 400 to 700 nm, being the main feature of the  $\text{Fe}_3\text{S}_4$  MCD spectrum, can be related to the excitation of the surface plasmon resonance (SPR) in the  $\text{Fe}_3\text{S}_4$  nanoparticles similar to that observed in the metal nanoparticles (de Heer 1993; Brack 1993; Kreibig and Vollmer 1995). It can be originated from the collective electron excitation induced by an applied electric field with a wavelength much larger than the particle size. These collective excitations are characterized by a finite life time and a certain frequency that differs substantially from the plasma frequency in the corresponding bulk material. As a result, the optical absorption spectra and magneto-optical effects are changed vs bulk sample, and the bands associated with the SPR excitation appear in visible spectral region. These bands can be wide enough due to the particles size dispersion.

## Conclusions

In summary, we reported the polyol mediated process approach for preparing several sets of the greigite  $\text{Fe}_3\text{S}_4$  nanoparticles with a different particle size and with low size dispersion within the set. The experimental results obtained by the X-ray powder diffraction, static magnetic measurements, and Mössbauer

spectroscopy have revealed the great effect of the technological conditions on the nanoparticles size, stoichiometry, and magnetic properties. According to the XRD data, the particles were characterized by the spinel-type structure with dimensions ranging from 9 to 20 nm depending on the Fe/S molar ratio and the heat treatment temperature and duration.

In small particles (about 9 nm), the Mössbauer spectroscopy revealed the occurrence of the nonstoichiometric phase of greigite with cation vacancies, whereas the stoichiometric phase of greigite  $\text{Fe}_3\text{S}_4$  dominates in the 18-nm-size nanoparticles. It was discovered that in small particles (<9 nm) all iron ions could be oxidized to ferric state and a vacant  $\gamma\text{-Fe}_2\text{S}_3$  spinel-type structure appears analogous to the oxide maghemite  $\gamma\text{-Fe}_2\text{O}_3$  structure. The superparamagnetic behavior of the  $\text{Fe}_3\text{S}_4$  particles was analyzed by the Mössbauer spectroscopy and magnetic measurements, and the blocking temperatures  $T_B \approx 230$  and 250 K were estimated for particles of 9 and 14 nm sizes, respectively. From the magnetic measurements the value of magnetic moment of the stoichiometric greigite nanoparticles was established to be about  $3.5 \mu_B$  per  $\text{Fe}_3\text{S}_4$  unit, which is higher than in bulk greigite ( $\approx 3.0 \mu_B$ ) found from neutron diffraction data (Chang et al. 2009).

A great degree of covalency in the Fe–S bonds of  $\text{Fe}_3\text{S}_4$  nanoparticles (known for bulk material) was established from the Mössbauer spectra parameters that support the fast electron  $\text{Fe}^{3+} \rightleftharpoons \text{Fe}^{2+}$  exchange in the B-sites of greigite. The absence of the Verwey transition at temperatures between 90 and 300 K is established supporting a semimetal type of conductivity.

The greigite magneto-optical properties are presented here for the first time in comparison with the MCD spectra of the  $\text{Fe}_3\text{O}_4$  thin film. The main information is obtained from the temperature and magnetic field dependences of the magnetic circular dichroism in the light wave length  $\lambda$  region between 300 and 1000 nm. The great difference between  $\text{Fe}_3\text{S}_4$  and  $\text{Fe}_3\text{O}_4$  magneto-optical properties was revealed. It is supposed that the MCD spectra of greigite nanoparticles result from the collective electron excitations in a wide band with superimposed peaks of the  $d\text{--}d$  transitions in Fe ions. Such behavior evidences the difference in electronic structure of these two allomeric compounds, and shows that MCD spectra can be considered as a decisive experiment when making choice between different theoretical models of the greigite energy structure.

**Acknowledgments** This work is supported by Russian Foundation for Basic Research (grant no. 11-02-92001) and the Russian Academy of Sciences under the Program “Nanotechnology and Nanomaterials” (grant no. 24-3.1). We also thank the National Science Council of Taiwan (NSC100-2923-M-218-001-MY3) for financial support.

## References

- Babinszki E, Márton E, Márton P, Ferenc Kiss L (2007) Widespread occurrence of greigite in the sediments of Lake Pannon: implications for environment and magnetostratigraphy. *Palaeogeogr Palaeoclimatol Palaeoecol* 252: 626–636
- Beinert H, Holm RH, Münck E (1997) Iron–sulfur clusters: nature’s modular, multipurpose structures. *Science* 277: 653–659
- Benning LG, Wilkin RT, Barnes HL (2000) Reaction pathways in the Fe–S system below 100°C. *Chem Geol* 167:25–51
- Brack M (1993) The physics of simple metal clusters: self-consistent jellium model and semiclassical approaches. *Rev Mod Phys* 65:677–732
- Chang L, Roberts AP, Tang Y, Rainford BD, Muxworthy AR, Chen Q (2008) Fundamental magnetic parameters from pure synthetic greigite ( $\text{Fe}_3\text{S}_4$ ). *J Geophys Res* 113:B06104
- Chang L, Rainford BD, Stewart JR, Ritter C, Roberts AP, Tang Y, Chen Q (2009) Magnetic structure of greigite ( $\text{Fe}_3\text{S}_4$ ) probed by neutron powder diffraction and polarized neutron diffraction. *J Geophys Res* 114:B07101
- Chang YS, Savitha S, Sadhasivam S, Hsu CK, Lin FH (2010) Fabrication, characterization, and application of greigite nanoparticles for cancer hyperthermia. *J Colloid Interface Sci* 363(1):314–319
- Chung A, Deen J, Lee JS, Meyyappan M (2010) Nanoscale memory devices. *Nanotechnology* 21. Article Number: 412001
- Coe JMD, Spender MR, Morrish AH (1970) The magnetic structure of the spinel  $\text{Fe}_3\text{S}_4$ . *Solid State Commun* 8: 1605–1608
- De Heer WA (1993) The physics of simple metal clusters: experimental aspects and simple models. *Rev Mod Phys* 65:611–676
- Dekkers MJ, Passier HF, Schoonen MAA (2000) Magnetic properties of hydrothermally synthesized greigite ( $\text{Fe}_3\text{S}_4$ ) II. High- and low-temperature characteristics. *Geophys J Int* 141:809–819
- Devey AJ, Grau-Crespo R, de Leeuw NH (2009) Electronic and magnetic structure of  $\text{Fe}_3\text{S}_4$ : GGA+U investigation. *Phys Rev B* 79:195126
- Fleet ME (1981) The structure of magnetite. *Acta Crystallogr Sect B Struct Sci* 37:917–920
- Fontijn WFJ, Van der Zaag PJ, Delivers MAC, Brabers VAM, Metselaar R (1997) Optical and magneto-optical polar Kerr spectra of  $\text{Fe}_3\text{O}_4$  and  $\text{Mg}^{2+}$ - or  $\text{Al}^{3+}$ -substituted  $\text{Fe}_3\text{O}_4$ . *Phys Rev B* 56:5432
- Gehring GA, Alshammari MS, Score DS, Neal JR, Mokhtari A, Fox AM (2012) Magneto-optic studies of magnetic oxides. *J Magn Magn Mater* 324:3422–3426
- Gleiter H (2000) Nanostructured materials: basic concepts and microstructure. *Acta Mater* 48:1–29

- Gubin SP, Koksharov YuA, Khomutov GB, Yurkov GYu (2005) Magnetic nanoparticles: preparation, structure and properties. *Russ Chem Rev* 74:489–520
- Hobbs D, Hafner J (1999) Magnetism and magneto-structural effects in transition-metal sulphides. *J Phys: Condens Matter* 11:8197–8222
- Hoffmann V, Stanjek H, Murad E (1993) Mineralogical, magnetic and Mössbauer data of symthite ( $\text{Fe}_9\text{S}_{11}$ ). *Stud Geophys Geod* 37:366–381
- Hunger S, Benning L (2007) Greigite: a true intermediate on the polysulfide pathway to pyrite. *Geochem Trans* 8:1–20
- Jaspersen SN, Schnatterly SE (1969) An improved method for high reflectivity ellipsometry based on a new polarization modulation technique. *Rev Sci Instrum* 40:761–767
- Jiang W-T, Horng C-S, Roberts AP, Peacor DR (2001) Contradictory magnetic polarities in sediments and variable timing of neoformation of authigenic greigite. *Earth Planet Sci Lett* 193:1–12
- Kreibig U, Vollmer M (1995) Optical properties of metal clusters. Springer, Berlin, p 23
- Kumar P (2010) Magnetic behavior of surface nanostructured 50-nm nickel thin films. *Nanoscale Res Lett* 5:1596–1602
- Kumar P, Krishna MG, Bhattacharya AK (2009) Effect of microstructural evolution on magnetic properties of Ni thin films. *Bull Mater Sci* 32:263–270
- Langford JJ, Wilson AJC (1978) Scherrer after sixty years: a survey and some new results in the determination of crystallite size. *J Appl Crystallogr* 11:102–113
- Lotgering FK (1964) Ferromagnetic interactions in ferromagnetic sulphides, selenides and tellurides with spinel structure. In: *Proceedings of international conference on magnetism*, Nottingham, p 533
- Lyubutin IS, Lin CR, Korzhetskiy YV, Dmitrieva TV, Chiang RK (2009) Mössbauer spectroscopy and magnetic properties of hematite/magnetite nanocomposites. *J Appl Phys* 106:034311
- Maher BA, Thompson R (eds) (1999) Quaternary climates, environments and magnetism. Cambridge University Press, Cambridge
- Makarov EF, Marfunin AS, Mkrtchyan AR, Nadzharyan GN, Povitskii VA, Stukan RA (1969) Mössbauer spectroscopic study of magnetic properties of  $\text{Fe}_3\text{S}_4$ . *Sov Phys Solid State* 11:391–392
- Menyah A, O'Reilly W (1991) The magnetization process in monoclinic pyrrhotite ( $\text{Fe}_7\text{S}_8$ ) particles containing few domains. *Geophys J Int* 104:387–399
- Morice JA, Rees LVC, Rickard DT (1969) Mössbauer studies of iron sulphides. *J Inorg Nucl Chem* 31:3797–3802
- Piekarz P, Parlinski K, Oles AM (2007) Order parameters in the Verwey phase transition. *J Phys Conf Ser (JPCS)* 92:012164
- Posfai M, Buseck PR, Bazylinski DA, Frankel RB (1998) Iron sulfides from magnetotactic bacteria: structure, composition, and phase transitions. *Am Miner* 83:1469–1481
- Roberts AP, Weaver R (2005) Multiple mechanisms of remagnetization involving sedimentary greigite ( $\text{Fe}_3\text{S}_4$ ). *Earth Planet Sci Lett* 231:263–277
- Roberts AP, Reynolds RL, Verosub KL, Adam DP (1996) Environmental magnetic implications of greigite ( $\text{Fe}_3\text{S}_4$ ) formation in a 3 m.y. lake sediment record from Butte Valley, northern California. *Geophys Res Lett* 23:2859–2862
- Roberts AP, Chang L, Rowan CJ, Horng C-S, Florindo F (2011) Magnetic properties of sedimentary greigite ( $\text{Fe}_3\text{S}_4$ ): an update. *Rev Geophys* 49:1–46. doi:[10.1029/2010RG000336](https://doi.org/10.1029/2010RG000336) (RG1002)
- Rowan CJ, Roberts AP (2006) Magnetite dissolution, diachronous greigite formation, and secondary magnetizations from pyrite oxidation: unravelling complex magnetizations in Neogene marine sediments from New Zealand. *Earth Planet Sci Lett* 241:119–137
- Skinner BJ, Erd RC, Grimaldi FS (1964) Greigite, the thio-spinel of iron; a new mineral. *Am Miner* 49:543–555
- Snowball I, Thompson R (1988) The occurrence of greigite in the sediments of Loch Lomond. *J Quat Sci* 3:121–125
- Snowball I, Thompson R (1990) A stable chemical remanence in Holocene sediments. *J Geophys Res* 95:4471–4479
- Spender MR, Coey JMD, Morrish AH (1972) The magnetic properties and Mossbauer spectra of synthetic samples of  $\text{Fe}_3\text{S}_4$ . *Can J Phys* 50:2313–2326
- Stanjek H, Murad E (1994) Comparison of pedogenic and sedimentary greigite by X-ray diffraction and Mössbauer spectroscopy. *Clays Clay Miner* 42:451–454
- Surerus KK, Kennedy MC, Beinert H, Münck E (1989) Mössbauer study of the inactive  $\text{Fe}_3\text{S}_4$  and  $\text{Fe}_3\text{Se}_4$  and the active  $\text{Fe}_4\text{Se}_4$  forms of beef heart aconitase. *Proc Natl Acad Sci* 86(24):9846–9850
- Uda M (1965) On the synthesis of greigite. *Am Miner* 50:1487–1489
- Vasilenko IV, Cador L, Quahab L, Pavlischuk VV (2010) Effect of production conditions on the size and magnetic characteristics of iron sulphide  $\text{Fe}_3\text{S}$  nanoparticles. *Theoret Exp Chem* 46:322
- Vasiliev I, Dekkers MJ, Krijgsman W, Franke C, Langereis CG, Mullender TAT (2007) Early diagenetic greigite as a recorder of the palaeomagnetic signal in Miocene–Pliocene sedimentary rocks of the Carpathian foredeep (Romania). *Geophys J Int* 171:613–629
- Verwey EJW (1939) Electronic conduction in magnetite  $\text{Fe}_3\text{O}_4$  and its transition point at low temperatures. *Nature* 144:327–328
- Wang J, Shi-He C, Wei Wu, Zhao G-M (2011a) The Curie temperature and magnetic exchange energy in half-metallic greigite  $\text{Fe}_3\text{S}_4$ . *Phys Scr* 83:045702
- Wang J, Gan JA, Wong YC, Berndt CC (2011) A review of preparation, properties and applications of rare earth magnetic thin films. In: Volkerts JP (ed) *Magnetic thin films: properties, performance and applications*. Series: Materials science and technologies condensed matter research and technology, Nova Science Publishers, pp 1–69. ISBN: 978-1-61209-302-4
- Yamaguchi S, Wada H (1973)  $\text{Fe}_2\text{S}_3$  of the spinel type structure with lattice defect. *Kristall und Technik* 8(9):1017–1019
- Zhang ZJ, Chen XY (2009) Magnetic greigite ( $\text{Fe}_3\text{S}_4$ ) nanomaterials: shape-controlled solvothermal synthesis and their calcination conversion into hematite ( $\alpha\text{-Fe}_2\text{O}_3$ ) nanomaterials. *J Alloys Compd* 488:339